Probing the X-ray and Radio emission of jetted sources

by

K. Maiti McGrath

A THESIS SUBMITTED IN PARTIAL FULFILMENT OF
THE REQUIREMENTS FOR THE DEGREE OF

BACHELOR OF SCIENCE

in

Honours Astrophysics

(Department of Astronomy and Physics, Dr. Luigi C. Gallo supervising faculty)

.....

.....

.....

.....

.....

SAINT MARY'S UNIVERSITY

June 24, 2021

Abstract

Probing the X-ray and Radio emission of jetted sources

by *K. Maiti McGrath*

submitted on June 24, 2021:

Five jetted sources are used in this work to probe the relationship between the X-ray and Radio emission from radio-loud active galactic nuclei. Timing techniques probing variability, light curve correlation, and power distribution are used to compare the two emission regimes. The power distribution, found using a structure function, showed some correlation with overall variability within the same emission regime, and also showed correlation between the power distribution of the different emission regimes. These correlations may indicate that the Radio and X-ray emission coming from these jetted sources are powered by the same processes.

Contents

List of Figures

List of Tables

Chapter 1

Introduction

Active Galactic Nuclei, or AGN, are found at the centre of galaxies and are the region around supermassive black holes (10^6 – 10^9 $M_\odot$). Though black holes are believed to be at the centre of most galaxies, only a fraction of these galaxies will host an AGN, where the black hole is actively accreting material. AGN are very bright and can outshine their host galaxies, emitting along most of the electromagnetic spectrum. These highly energetic objects may also host a jet, a galactic scale event of collimated matter from the black hole region. Figure 1.1 highlights the difference in scale of the AGN itself and the jet that outflows from it. The black hole and disk region are typically about the size of our solar system, and the jets typically extend past the host galaxy and to the spaces between galaxies.

1.1 AGN and Jets

The components in AGN are similar (Figure 1.3) though jets appear less common. The black hole at the centre is actively accreting material from the accretion disk, which is swirling around the black hole. The material in the accretion disk is hot and emits from the X-ray through the UV to the Optical regimes. Above the black hole and the accretion disk exists the corona, a hot cloud of electrons. The jets, when present, out-flow along the spin axis of the black hole, generally perpendicular to

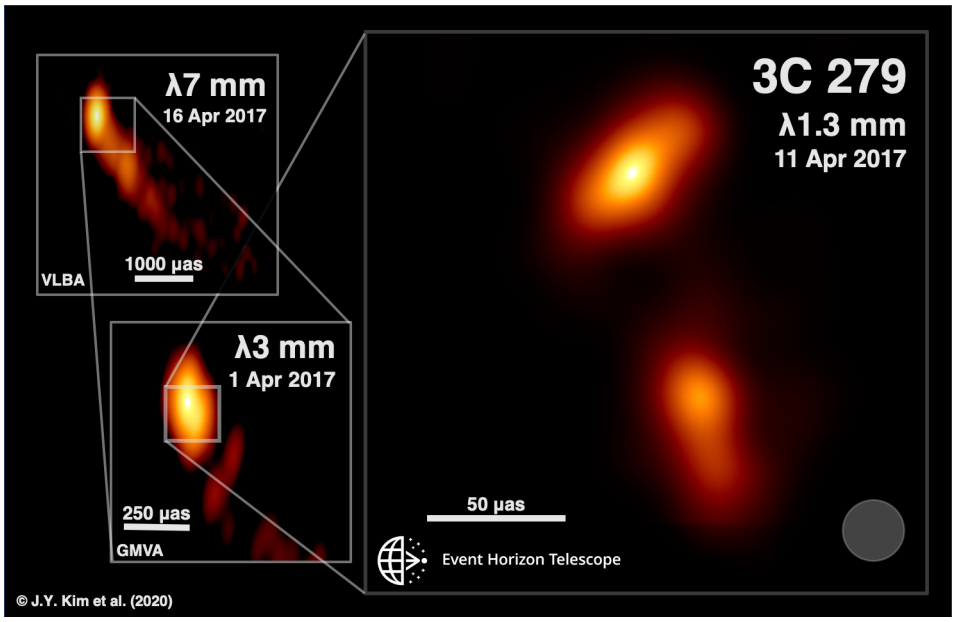

Figure 1.1: Image from J. Y. Kim et al. (2020) showing the AGN called 3C279 and its jet, with scale markings ranging from 1000-50 micro arc-seconds, showing that the jet is much larger than the central region of the disk and the black hole.

the accretion disk. Emission from the jet covers a large range of the electromagnetic spectrum from X-rays to Radio, with the higher energy emission coming from the base of the jet and the lower energy emission coming along the jet, even gamma-ray emission is sometimes present in jets.

The X-ray emission comes from a few different sources in the AGN. In most, this emission comes from the accretion disk and the corona. The accretion disk is made of hot material and thermally emits as a black body in the optical, UV and X-ray regimes. Around supermassive black holes, the accretion emission peaks in the UV, so most of the emission coming from it is at this energy. The emission from the accretion disk close to the black hole may go through the corona and Compton up-scatter to higher energy emission. Compton up-scattering occurs when low-energy photons (UV) enter the corona and collide with the high energy electrons (Gallo

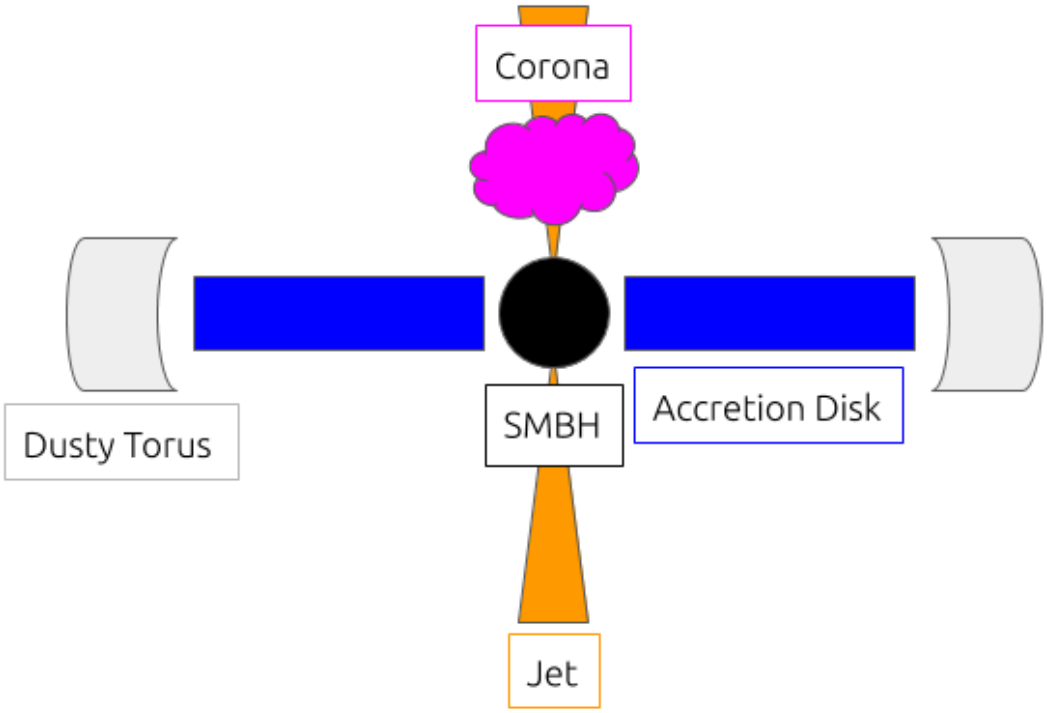

Figure 1.2: Diagram showing the regions of an AGN. The X-ray emission comes from the accretion disk (blue) and the corona (pink) and the base of the jet (orange). The Radio emission originates at large distances from the jet base.

2011). Energy is transferred from the electron to the photon during the collision. The photon continues to collide with electrons and gain energy until it scatters out of the corona. Due to the Compton scattering, the corona re-emits the higher energy photons isotropically. Figure 1.3 illustrates this emission and re-emission process.

X-ray emission can also come from processes in jets. Jets are collimated, charged matter that is out-flowing from the central region of the black hole and accretion disk. The strength of a jet depends on the magnetic field of the AGN among other intrinsic properties, like black hole mass and spin (Blandford et al. 2019). The matter in the jet is charged and is moving through the magnetic field present in the AGN. The charged particles are accelerated at relativistic velocities and are emitting

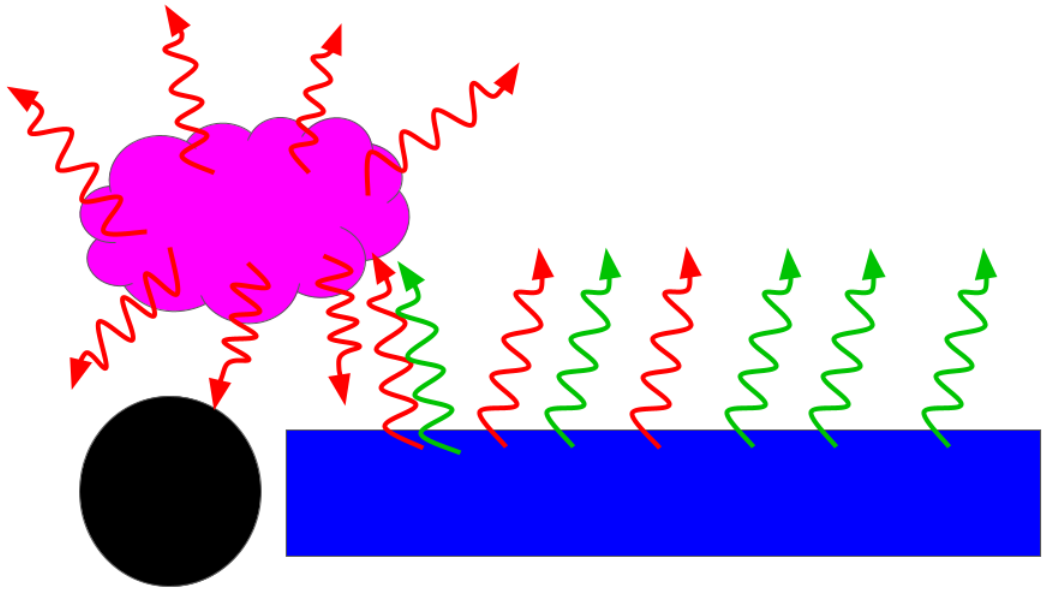

Figure 1.3: Diagram showing the X-ray emission (red) from AGN. X-rays and UV rays (green) are emitted from the accretion disk (blue) and some of this emission is up-scattered by the corona (pink) into another source of X-ray emission.

synchrotron radiation along the jet. Radio emission in these sources comes from synchrotron radiation along the jet. The X-ray synchrotron emission comes from the area near the base of the jet where the particles are more energetic and the magnetic field is stronger. This collimated material is not uniform and has some regions that are more dense than other regions. These dense regions are referred to as knots and are radiating through synchrotron self-Comptonization (Marscher 2006). The high density of material increases the likelihood of collisions. As the photons are emitted from synchrotron radiation they are Compton up-scattered by another moving particle. The synchrotron and the synchrotron self-Compton radiation are both sources of X-rays. There is also speculation that radiation from the Cosmic Microwave Background (CMB) could also be up-scattered by the knots in the jets, this process is

called external Comptonization since the photons originate externally from the jet and the AGN. Figure 1.4 gives a general physical illustration of the X-ray and Radio emitting regions in a jet.

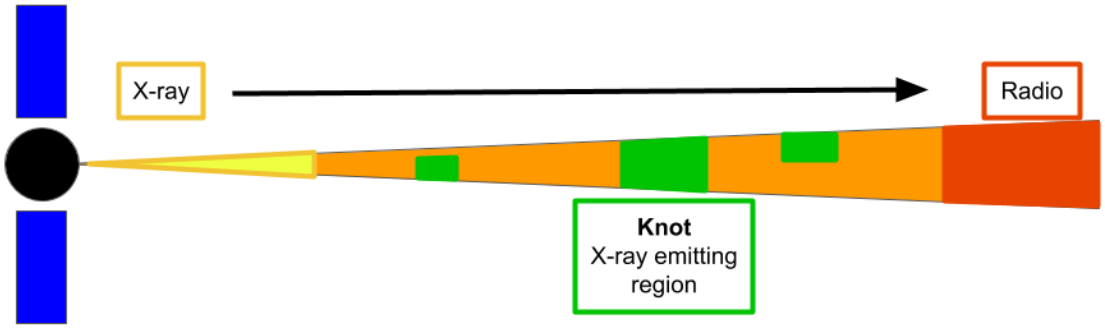

Figure 1.4: Sketch adapted from Marscher (2006) showing the emission regions in a jet (orange). The Synchrotron X-ray (yellow) and Radio (red) emission regions are shown as well as some examples of knots (green) where X-ray synchrotron self-Compton emission occurs.

1.2 Variability Properties

Some AGN are known for being highly variable. A source that is able to vary on timescales from hours to years makes for some interesting observations. Observing variability properties can be used to probe many things about an AGN, due to the emission coming from varying regions. Some variability properties can give insight into the size of regions, the distance between regions, and in some cases can show correlations between inherent AGN properties and observed processed variability. This work will use excess variance, reverberation mapping, and structure functions to probe different variability properties in radio loud, jetted sources.

1.2.1 Excess Variance

Excess variance is a way of measuring variability in a light curve. It quantifies the variability amplitude in a light curve. With excess variance we can examine "bins" or time segments of light curves to show how the variability changes on different time scales. Following the methods outlined in Ponti et al. (2012) the calculation used for the normalised excess variance is

$$\sigma_{rms}^2 = \frac{1}{N\mu^2} \sum_{i=1}^{N} [(X_i - \mu)^2 - \sigma_i^2] \tag{1.1}$$

where N is the number of bins, μ is the unweighted mean of the counts in each bin, X_i and σ_i are the count rate and uncertainty, respectfully, of each bin.

Ponti et al. (2012) studied the excess variance of radio quiet sources and found significant correlations, notably with the mass of the black hole and the accretion rate. Figure 1.5 shows the correlation that they found between the excess variance at different timescales with the mass. The fit for these plots are all very similar regardless of timescale, showing that generally higher mass black holes show lower variability at all variable timescales. They also found a positive correlation between the excess variance of the high energy X-rays and the excess variance of the low energy X-rays for their sources (Figure 1.6). This correlation is found at different timescales and is similar across the timescales shown, thus showing the variability at different energies and timescales are related in the sources, possibly being produced by the same processes across the sources.

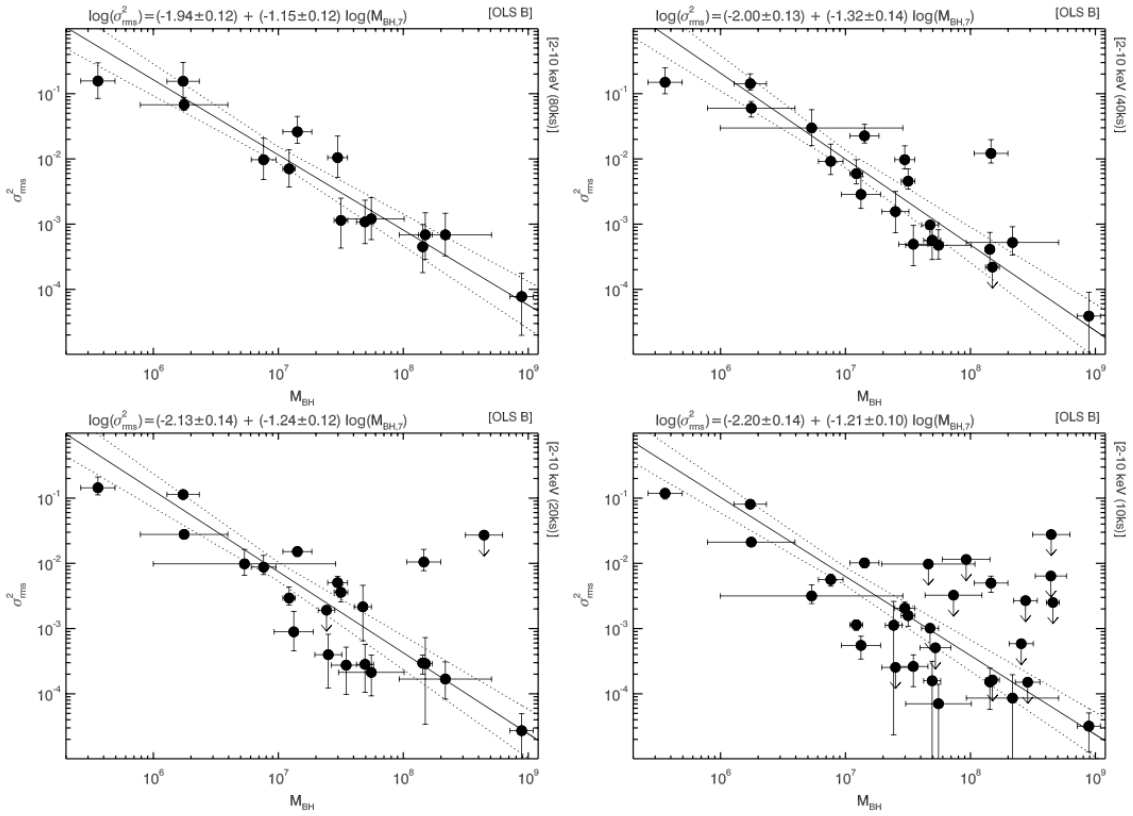

Figure 1.5: Figure 3 from Ponti et al. (2012), shows the excess variance, on the y-axis, against the mass. The plots are of the excess variance of different timescales, 80, 40, 20, and 10ks in the top left, top right, bottom left, and bottom right respectively.

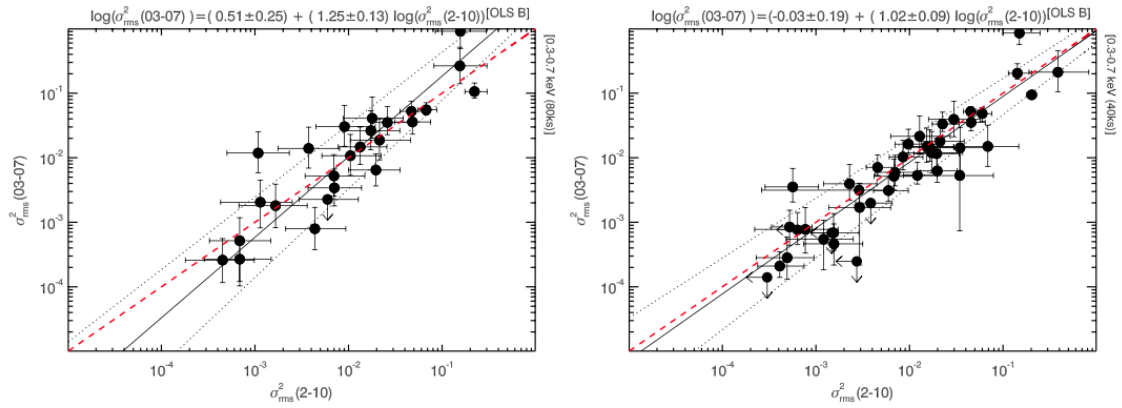

Figure 1.6: Figure 2 from Ponti et al. (2012), shows the excess variance of the lower energy X-rays, on the y-axis, against the excess variance of the higher energy X-rays. The plots are of the excess variance of different timescales, 80ks bins on the left and 40ks bins on the right.

1.2.2 Reverberation Mapping

Reverberation mapping is a technique that uses light curves from two different regions of an AGN and attempts to find similar patterns in both light curves, or a correlation between the two. If a correlation is found, it might be that there is a delay between the signals. This is sometimes referred to as a time lag or simply a lag, and it can give information on the AGN processes occurring.

The technique was made famous in optical astronomy to compare correlations between the continuum and the broad line region (BLR) light curves. Peterson (1993) used reverberation mapping to probe the spatial area of the BLR, with the results allowing them to get insight into the shape, size, and kinematics of the BLR. Reverberation mapping has also been used to calculate the mass of the black hole. Peterson (2014) discusses the ways in which reverberation mapping can be used to do that. In some cases scaling relationships were used to indirectly measure the mass, whereas others used the spatial resolution to confine the central region of the AGN and measure physical features of the BLR affected by the gravitational force of the black hole mass.

The lag found between the light curves can indicate the physical distance between the emission regions, or a disturbance in a process which propagates from one region to the other. In this work, looking at X-rays and Radio emission, the most likely propagation we will be able to probe is some kind of propagation along the jet. A lag between X-ray emitting region at the base of the jet and the Radio emitting region at the far end of the jet would be able to give information over a significant portion

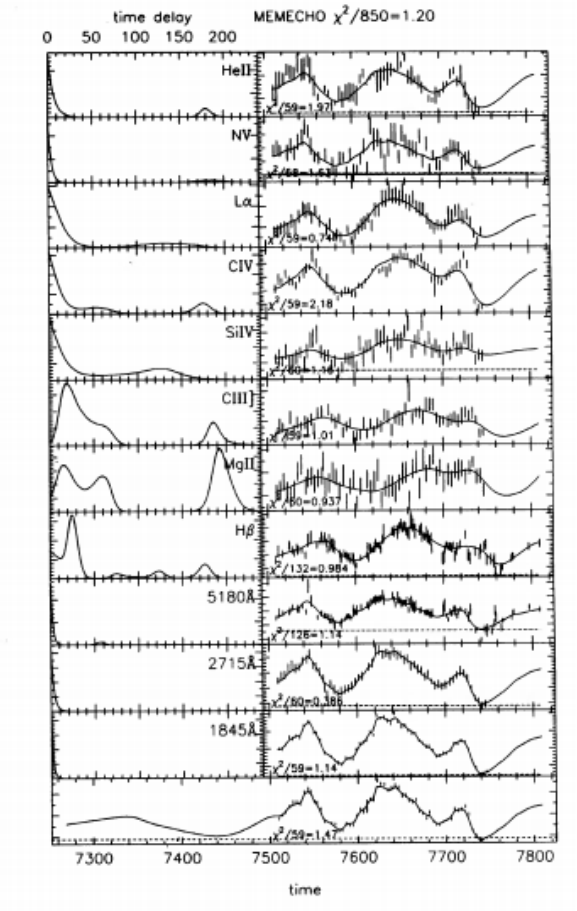

Figure 1.7: Figure 5 from Peterson (1993). The right side shows the light curve of different emission lines in the UV and optical, compared to the continuum light curve (bottom) for NGC 5548. The panels on the left show the correlation with an applied time lag.

of the jet. Alternatively, if correlations are seen without lag, then the emission could be from a knot. This work will be using a program called JAVELIN (Zu et al. 2011) that searches for correlations and lags between light curves.

1.2.3 Structure Function

A structure function is another way of calculating a power spectral density (PSD), which shows the distribution of power in a light curve at different frequencies. A

structure function differs by operating in the time domain rather than the frequency domain but they provide similar information. This difference allows data that has more irregular sampling to be treated without the issues that arise from Fourier based PSD calculations.

This work uses the structure function program developed by Gallo et al. (2018), and in their work they explore the meanings of different slopes and characteristic timescales. Figure 1.8 shows some of the structure function plots from their work and it highlights what a typical structure function looks like. Their work found similarities in the distribution of power in the optical and UV light curves of an AGN called Mrk 335.

This work hopes to be able to use structure functions as a way to determine if there is a correlation between the X-ray and Radio emission in radio loud AGN.

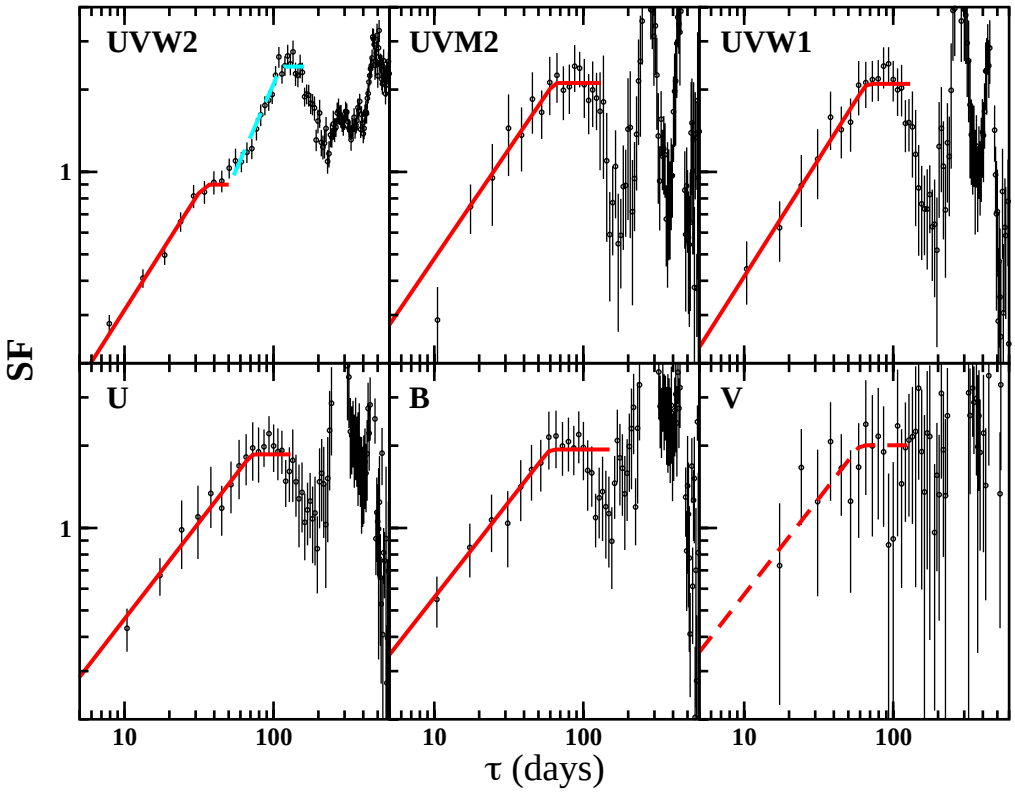

Figure 1.8: Figure from Gallo et al. (2018) showing the UV band structure functions of Mrk 335. The typical structure function is shown in bands UVM2, UVW1, U, B, and V, where the initial data can be fitted by a power law and then flattens out before becoming noise dominated. UVW2 shows a non-typical structure funtion where there are two characteristic timescales found where the slope of the power law flattens out.

1.3 XRT, RXTE, and OVRO

The telescopes used to collect the data used in this work are the *Swift XRT* (Evans et al. 2007, Evans et al. 2009), the *RXTE* (Rivers et al. 2013), and the *Owens Valley Radio Observatory (OVRO)* 40m telescope (Richards et al. 2011).

The *Swift* telescope was launched in 2004 with the aim of studying gamma-ray burst events. *Swift* is a multi-wavelength observatory with observing capabilities in the UV and Optical bands as well as X-ray and gamma-ray. The X-ray telescope, XRT, on *Swift* is sensitive from 0.3-10 keV. The data used in this work comes from this instrument but to match the other set of X-ray data only energies 2-10 keV were used. *Swift* remains active and continues to collect data.

The Rossi X-ray Timing Explorer, *RXTE*, was launched in 1995 and remained active until its decommission in 2012. While it was active it was used to study black holes, neutron stars, and X-ray pulsars. *RXTE* was especially used for highly variable sources as it was a timing mission, and was able to have data distinguished down to microseconds. *RXTE* also offers a large energy range for data to be taken, with a range from 2-200 keV, though the data used in this work will be at energies 2-10 keV using the Proportional Counter Array, PCA, instrument.

The *OVRO* 40m telescope is sensitive at 15GHz and started as a part of the Very Long Baseline Interferometer in 1968 and stayed as part of that project until 1991 when the Very Long Baseline Array launched and came on line. In 2008 the 40m telescope started a blazar monitoring program, where the goal was to investigate jetted AGN to learn more about the formation and composition of jets, the magnetic

fields present in jetted AGN, and the process by which the particles are ejected and how they emit. The monitoring program is still active currently and regularly observes a myriad of jetted AGN sources.

1.4 Motivation

The goal of this work is to look at different variability processes in jetted radio loud AGN and determine if there are significant correlations between these values and intrinsic properties of the sources. This type of study has been done on radio quiet sources so this work is looking to do a comparable study with jetted radio loud sources. The variability in these sources could also give insight into the processes at work, and if they affect each other or are connected. Synchrotron, synchrotron self-Compton, and inverse Compton radiation could all contribute to the emission coming from these sources, and looking at the variability may let us distinguish which processes are at work; if there is only one process dominating or if they are all present at some level.

Chapter 2

Sample and Data

2.1 Sample

The sources chosen for this project depended on available data from archival sources. The *OVRO* and *RXTE* databases were selected and the overlapping sources were found through coordinate and name matching. This yielded approximately 40 sources that appeared in both archives. The *OVRO* database had some sources that were listed but did not have data available to the public, so this eliminated some potential sources. With the remaining sources, the light curves from the *RXTE* database were checked for satisfactory sampling. This eliminated many sources who had well sampled but short light curves and sources that had light curves that spanned a large time frame but were sparsely sampled. This left five sources, 3C 273, 3C 279, 3C 120, Mrk 421, and NGC 1052.

2.2 Sources

Table 2.1 lists the sources, duration of the observations of that source, and the number of observations taken by each telescope. The overlapping dates for the X-ray observations and the Radio observations are generally from 2008 to 2020, aside from 3C 120 whose *XRT* observations stop in 2017. The sampling taken with *OVRO* is

largely consistent for each source, where the X-ray observations show more variance.

Source Name	Radio Type	Telescope	Dates observed	Number of observations
3C 120	Flat-Spectrum Radio Source	XRT	03-28-2007 - 03-28-2017	161
		RXTE	03-11-1996 - 05-01-2007	1335
		OVRO	01-09-2008 - 06-14-2020	627
3C 273	Flat-Spectrum Radio Source	XRT	02-17-2005 - 07-07-2020	269
		RXTE	02-02-1996 - 12-31-2011	1960
		OVRO	01-08-2008 - 06-21-2020	786
3C 279	Flat-Spectrum Radio Source	XRT	01-13-2006 - 03-20-2020	7852
		RXTE	01-22-1996 - 12-30-2011	1987
		OVRO	01-08-2008 - 06-21-2020	607
Mrk 421	Flat-Spectrum Radio Source	XRT	03-01-2005 - 11-08-2020	1072
		RXTE	03-01-1996 - 12-31-2011	1182
		OVRO	01-08-2008 - 06-30-2020	842
NGC 1052	Flat-Spectrum Radio Source	XRT	01-19-2007 - 01-28-2020	806
		RXTE	06-06-2005 - 12-27-2009	148
		OVRO	01-06-2008 - 05-31-2020	589

Table 2.1: Table showing the sources and their radio classification, the range of observation dates for each telescope (listed month-day-year), and the number of observations taken.

Chapter 3

Timing Techniques

The timing techniques used in this study are excess variance, reverberation mapping, and the structure function. These timing techniques are able to investigate different regions and variability from the sources. Excess variance is able to show the difference in variability between the Radio and X-ray regimes of a source. Reverberation mapping looks to find any correlation between the light curves of the Radio and X-ray, and the structure functions, like a power spectral density, shows the power output over a range of timescales for a source in the different emission regimes.

The X-ray light curves used for the reverberation mapping and structure function calculations were combined versions of the *XRT* and *RXTE* light curves. Both were normalized to their average and then combined by their MJD values. This was done to fill gaps in the X-ray light curves to increase quality and extend them to longer timescales (Figure 3.1).

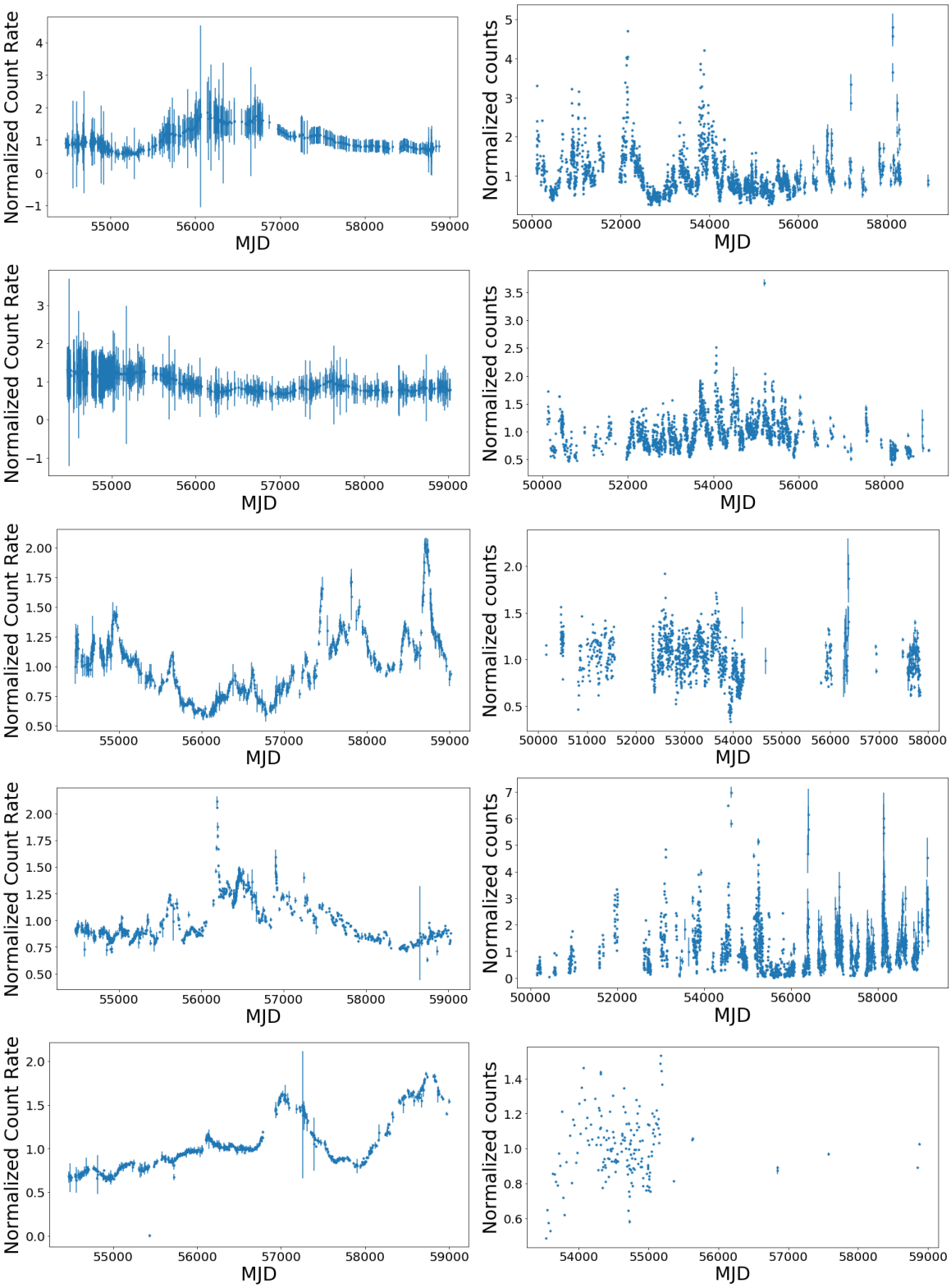

Figure 3.1: Light curves of the X-ray (right), and Radio (left) for each source. From top to bottom the sources are 3C 279, 3C 273, 3C 120, Mrk 421, and NGC 1052. All the light curves are normalized to their average, and the time is given in MJD.

3.1 Excess Variance

Excess variance is a widely used technique to describe the variability in the emission from a source, and has been found to show some correlations with different parameters in AGN (Ponti et al. 2012). In this work, the equation given in Ponti et al. (2012) was used to calculate both the excess variance of the light curves and the errors. The excess variance was calculated for different timescales for each light curve. Each light curve was more than 10 years long and so the divisions used were half year, one year, five years, and 10 year sections for the light curves. These values were then plotted against time to see if there were any correlations and none were found. The average Radio and X-ray excess variances for all timescales were plotted (Figure 3.2). This shows the relative variability of the two emission regimes. In some cases, the standard deviation of the many excess variance values were used to give insight into the spread of the values for a certain time length.

For almost all the sources, the X-ray variability was stronger than the Radio variability at all timescales, the exceptions had stronger radio variability only on the shorter timescales. These can be seen in Figure 3.2, in which 3C 120 and NGC 1052 both have higher variability in Radio at the longer timescales. This general trend is expected when considering the potential sizes of the two emission regions: X-ray emission from the disk and the central region is coming from a smaller area than the Radio emission which is coming from somewhere along the jet. The jet is typically orders of magnitude larger than the disk and central region.

When comparing the timescales, the longer timescales are more variable than the

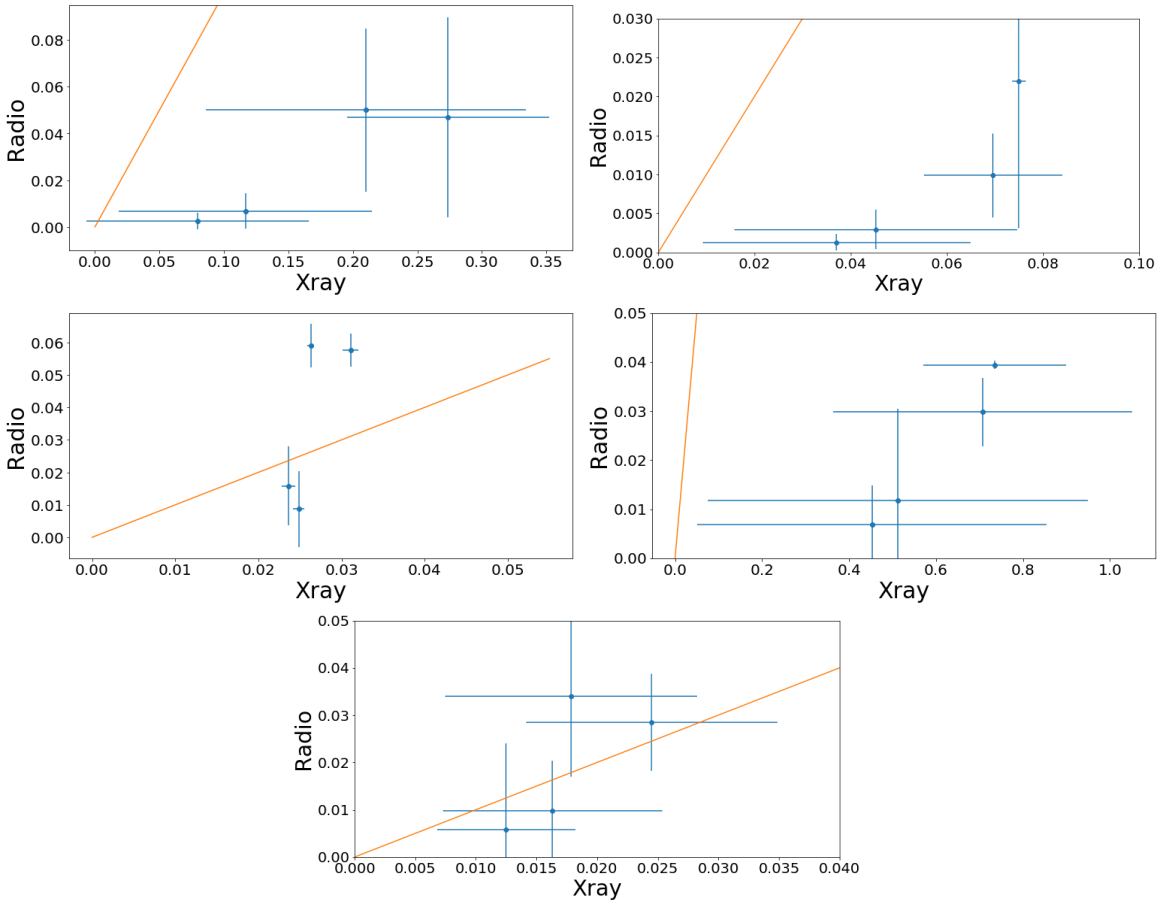

Figure 3.2: Excess variance of each source. The radio values are plotted against the X-ray values, with each point being a different timescale. The sources are 3C 279 (top left), 3C 273 (top right), 3C 120 (middle left), Mrk 421 (middle right), and NGC 1052 (bottom). The orange lines through each panel show a line through 0 with a slope of 1.

shorter timescales for both the Radio and X-ray emission. This can be seen in every panel in Figure 3.2, where the two data points with higher variability are the points for 5 year and 10 year binning. This is also an expected result, as there is more opportunity for variability to occur over large timescales, and shorter timescales may not grasp a general change in variability since the change happens over a larger time than the binning. Larger binning allows for short and long term variability to be detected whereas shorter binning will detect only variability on shorter timescales.

Source Name	Band	0.5 year bins	1 year bins	5 year bins	10 year bins
3C 120	X-ray	0.0249 ± 7e-4	0.0236 ± 8e-4	0.0263 ± 4e-4	0.031 ± 1e-3
	Radio	0.01 ± 1e-2	0.02 ± 1e-2	0.059 ± 6e-3	0.058 ± 5e-3
3C 273	X-ray	0.04 ± 3e-2	0.05 ± 3e-2	0.07 ± 1e-2	0.075 ± 1e-3
	Radio	0.001 ± 1e-3	0.003 ± 2e-3	0.010 ± 5e-3	0.02 ± 2e-2
3C 279	X-ray	0.08 ± 9e-2	0.1 ± 1e-1	0.2 ± 1e-1	0.27 ± 8e-2
	Radio	0.003 ± 4e-3	0.007 ± 8e-3	0.05 ± 3e-2	0.05 ± 4e-2
Mrk 421	X-ray	0.5 ± 4e-1	0.5 ± 4e-1	0.7 ± 3e-1	0.7 ± 2e-1
	Radio	0.007 ± 8e-3	0.01 ± 1e-2	0.030 ± 7e-3	0.0394 ± 8e-4
NGC 1052	X-ray	0.013 ± 5e-3	0.016 ± 9e-3	0.02 ± 1e-2	0.02 ± 1e-2
	Radio	0.006 ± 2e-2	0.01 ± 1e-2	0.03 ± 1e-2	0.03 ± 2e-2

Table 3.1: Table of the excess variance calculated for the different time bins for each source.

3.2 Reverberation Mapping

Reverberation mapping is used to find any correlations between light curves. The method used in this work was a program called JAVELIN created by Zu et al. (2011) as a way of mapping any reverberations, also known as lags, between the emission line and continuum light curves of an AGN.

The *RXTE* and *XRT* X-ray light curves were combined to create a longer and higher quality light curve. Using this X-ray light curve along with the corresponding *OVRO* light curve for the source they were entered into the program which ran a Monte Carlo Markov Chain (MCMC) which stepped through different smoothing, normalization, and time lag parameters. The program's smoothing parameter adjusts the light curves slightly in order to facilitate finding correlations. The light curves are smoothed, so some of the smaller variations are lessened to show a more general shape of the light curve which will be more easily compared. The normalization parameter shifts the second light curve, being compared to the first, so that when

they are compared they overlap more directly. The lag parameter is the shift along the time axis that looks to find the strongest correlation between the light curves. The shift can be positive or negative, which would show whether the first light curve is leading the change in emission or if the second light curve is leading.

The program returns a histogram of the values for these parameters; the one of interest for this work is that of the time lag (Figure 3.3). The histogram is used to show areas where the program has found a possible correlation of the light curves at these points.

The results from the reverberation mapping showed that none of the sources showed any significant correlation in the light curves. In Figure 3.3 there are no large spikes in the histograms. A spike would indicate that a correlation was found at that time lag multiple times through the MCMC runs. While we expected to find a correlation initially, the lag time may be longer than 10 years which is the average size of the light curves, in this case a correlation would not be detected with the data that we have at this time. The emission regions themselves may not affect each other which would also not show a correlation between the light curves. The program itself would often find some small number of MCMC runs with a correlation, but these lag times corresponded with the light curves being moved completely to the end of the other. Instead of overlapping the similar emission patterns in the light curves, they were moved so no part of the light curve overlapped. This was erroneously found by the program to be a correlation and these results were rejected.

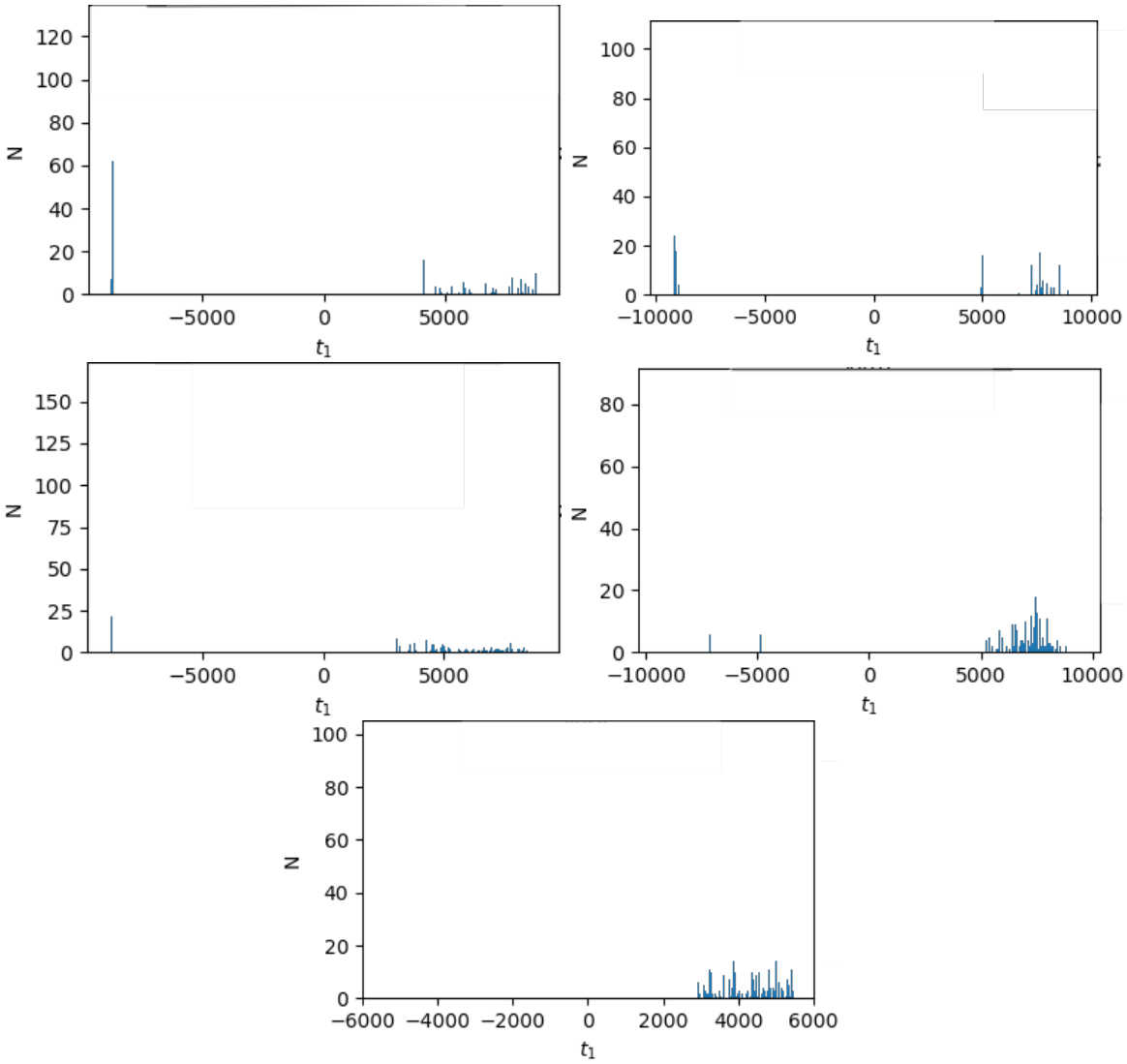

Figure 3.3: Histograms showing the lag time at which an MCMC run found a correlation between the X-ray and Radio light curves. 5000 days is approximately 13.5 years. The sources are 3C 279 (top left), 3C 273 (top right), 3C 120 (middle left), Mrk 421 (middle right), and NGC 1052 (bottom).

3.3 Structure Function

Structure functions are very similar to power spectral densities (PSDs) the primary difference being that the structure function works in the time domain where a PSD works in the frequency domain. This method was used in Gallo et al. (2018) and the same method was used in this work, with the same programming package. The

previous work done for Gallo et al. (2018) was compiled into a downloadable python package available online and can be used to make structure functions from a given light curve. This method was more favourable than a traditional PSD as this method is able to handle more gaps in the light curves and return the results, whereas a traditional PSD will not be able to manage having many gaps or long gaps in a light curve and will not produce anything of use. The structure function was also done with the combined X-ray light curve to fill in gaps and enhance the quality.

In previous works, structure functions and PSDs for X-ray light curves have been fit with a broken power law with the first index free to vary and the second index fixed to zero (Gallo et al. 2018). The break frequency, or characteristic frequency, is the point where the power law changes from the first to the second. In this work, the output is in terms of time rather than frequency so the break is in terms of time. All the structure functions were fit with a broken power law where the first index and the break time were left to vary.

The characteristic timescales for the Radio breaks are similar, with a notable outlier with NGC 1052 (Figure 3.4), which had a particularly variable structure function. The indices for the Radio are also similar but Mrk 421 has a higher value than the rest, which may be a result of the lack of small timescale values in the structure function.

The characteristic timescales for the X-ray breaks are all similar, aside from Mrk 421 which is significantly lower than the rest (Figure 3.5), possibly due to the flat shape of the structure function compared to the other X-ray structure functions. All the X-ray indices are similar to each other.

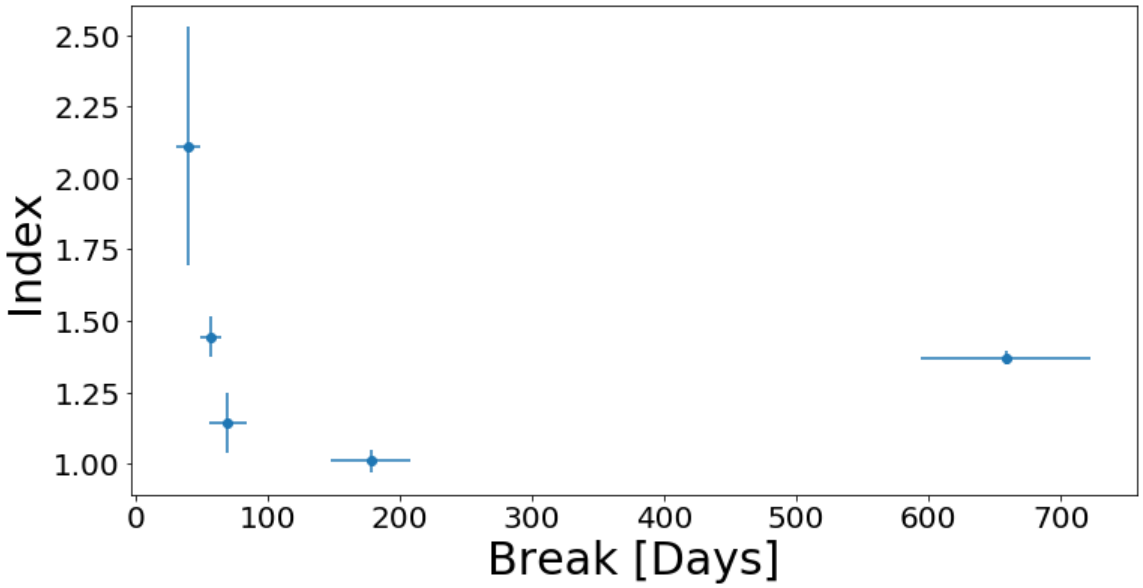

Figure 3.4: Radio structure function index against the structure function break for each source. The outlier to the right of the plot is NGC 1052.

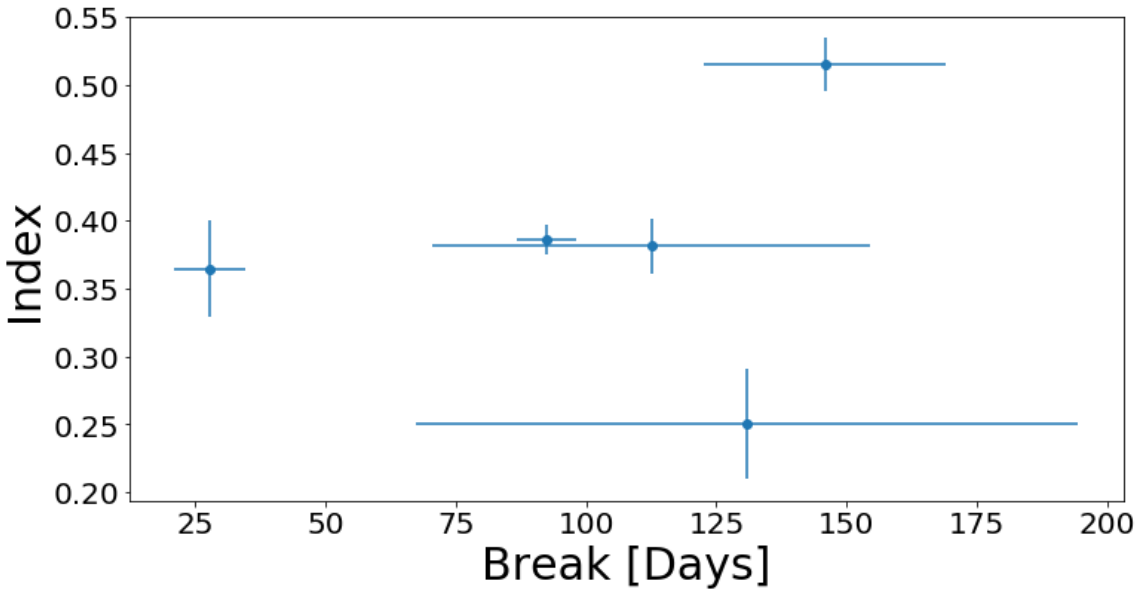

Figure 3.5: X-ray structure function index against the structure function break for each source. The outlier to the left of the plot is Mrk 421.

Similarities in the structure function, of the index or of the break time, could indicate that the processes producing these results is the same for the different sources. Differences in values could indicate the opposite, that the processes are not the same or could be a consequence of the simple model used to fit the structure functions. Several of the structure functions exhibited structures that appeared to show multiple breaks, our model does not account for more than one break time. The quality of the data may also affect the effectiveness of the model used to interpret the data. If there were a break that was hidden because of insufficient sampling at that timescale, a different process may appear more obvious at a longer timescale and would be different from the other sources.

Source Name	Band	Break	Index
3C 120	X-ray	93 ± 17	0.39 ± 1e-2
	Radio	70 ± 33	1.1 ± 1e-1
3C 273	X-ray	142 ± 33	0.51 ± 2e-2
	Radio	178 ± 30	1.01 ± 4e-2
3C 279	X-ray	113 ± 57	0.38 ± 2e-2
	Radio	57 ± 8	1.44 ± 7e-2
Mrk 421	X-ray	28 ± 17	0.36 ± 4e-2
	Radio	40 ± 20	2.1 ± 4e-1
NGC 1052	X-ray	130 ± 49	0.25 ± 4e-2
	Radio	659 ± 64	1.37 ± 3e-2

Table 3.2: Table showing the structure function break time, in days, and the index of the model fit to each structure functions per source.

Chapter 4

Radio and X-ray timing properties of the sample

4.1 Excess Variance

The excess variance of the sources were calculated and are shown plotted per source and averaged of all the sources, in Figure 4.1. The calculated X-ray values for the excess variance were typically larger than those in the Radio, as expected since the emission region for X-rays is smaller than the Radio emission region. A smaller region is able to change faster than a large region, thus meaning the emission from a smaller region will also change faster than the emission coming from a larger region.

There were two sources where the longer timescales were more variable in the Radio than they were in the X-ray, these sources were NGC 1052 and 3C 120. The Radio light curves for both these sources show more variability in emission, possibly showing a change in continuum emission for the sources at specific points in time. If the continuum emission is fluctuating only in these sources that could explain why the Radio variability is higher than the X-ray variability at longer timescales.

The longer timescales were more variable for both the X-ray and the Radio for all sources (see Chapter 3.1). This was an expected outcome and Figure 4.1 shows the average over all sources of each time bin plotted. The longer timescales (5 year and

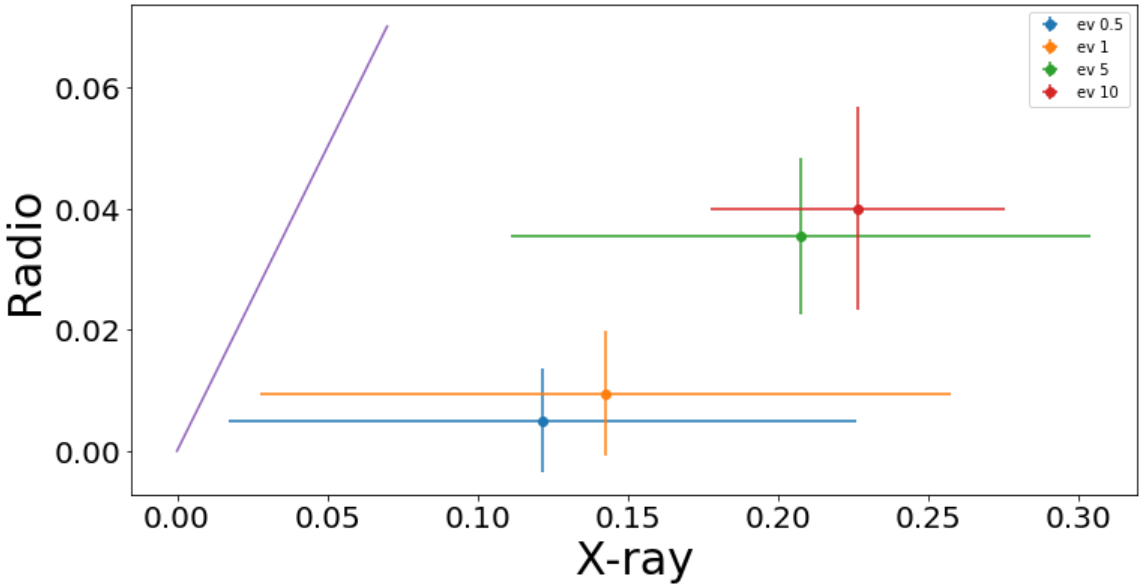

Figure 4.1: Plot showing the excess variance of the Radio and X-ray light curves at 0.5 (blue), 1 (orange), 5 (green), and 10 (red) year intervals. A line with a slope of 1 is shown in purple. The error bars are a standard deviation of the averaged values.

10 year bins) are distinct from the two shorter timescales (0.5 year and 1 year bins). This plot also shows that on average, for these sources, the X-ray emission is more variable than the Radio emission.

4.2 Structure Function

Fitting the structure functions provided the break time of the sources and the index of the initial power law. The break times of the X-ray and Radio regimes, when plotted against each other seem to show a possible positive correlation (Figure 4.2). The line shown in the figure is a line with slope 1 fit through the origin, showing a 1 to 1 relationship. The outlying source is NGC 1052 and is the source among them with the poorest data quality and most sparseness. The structure function for NGC 1052 may show more detail if more data is added to the light curves. Increasing the quality of the data may show a break that is currently undetectable in a significant way.

The indices of the two regimes are also plotted, and show a possible negative correlation (Figure 4.3). This plot also shows a single source as an outlier, but in this case it is Mrk 421. The Radio structure function for Mrk 421 has a much more variable structure compared to the others. Its unique shape has the typical broken power law shape but appears to show more possible breaks before the data becomes dominated by noise. Both the Radio and the X-ray index values have large error bars and could indicate that the model used to fit the structure functions is not robust enough.

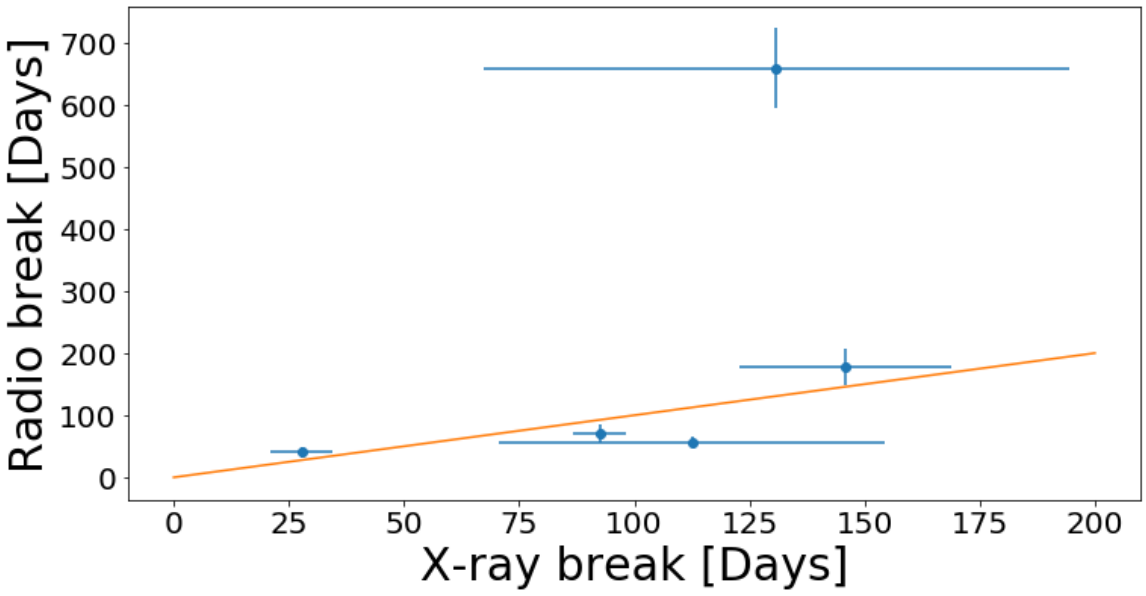

Figure 4.2: Plot showing the break time of the Radio and X-ray structure functions of each source. The break time is given in days and the orange line denotes a line of slope 1 that goes through the origin. The outlying source is NGC 1052.

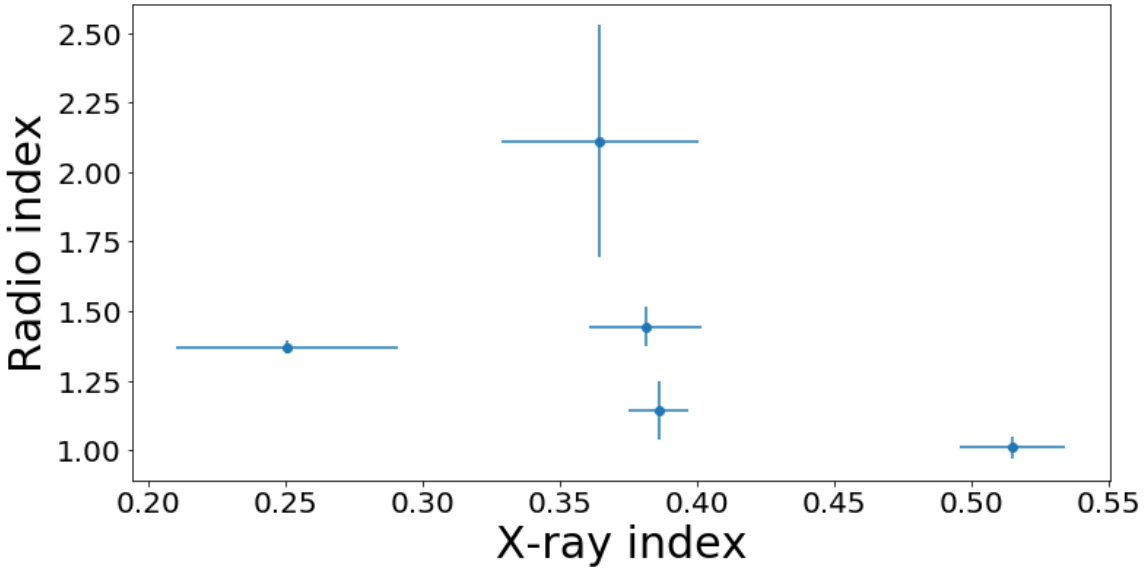

Figure 4.3: Plot showing the index of the Radio and X-ray structure functions of each source. The outlying source is Mrk 421.

4.3 Cross Correlations

There were many correlations found between the X-ray and Radio results from each of the timing techniques and there were also some that appeared comparing the X-ray timing techniques and the Radio timing techniques. Comparing the excess variance at half year steps and the structure function breaks revealed potential correlations between these parameters. These two parameters are compared since the break times are most similar with the timescale of the half year excess variance so a correlation was probably more likely to be visible between these parameters. (See Figures 4.4 and 4.5)

The X-ray excess variance against break time (Figure 4.4) shows a potential visual correlation between the two X-ray parameters. Figure 4.5 has the same parameters compared but in the Radio regime. The leftmost points in Figure 4.5 show a possible negative correlation. NGC 1052 has been identified as an outlier for the Radio break values and appears again as an outlier in this figure.

These two correlation plots have not been fit. In the future after they are fit, comparing the fit parameters between the X-ray and Radio would be interesting. Comparing the parameters may give insight as to whether the process affecting the excess variance and the break time are the same for both the X-ray and Radio.

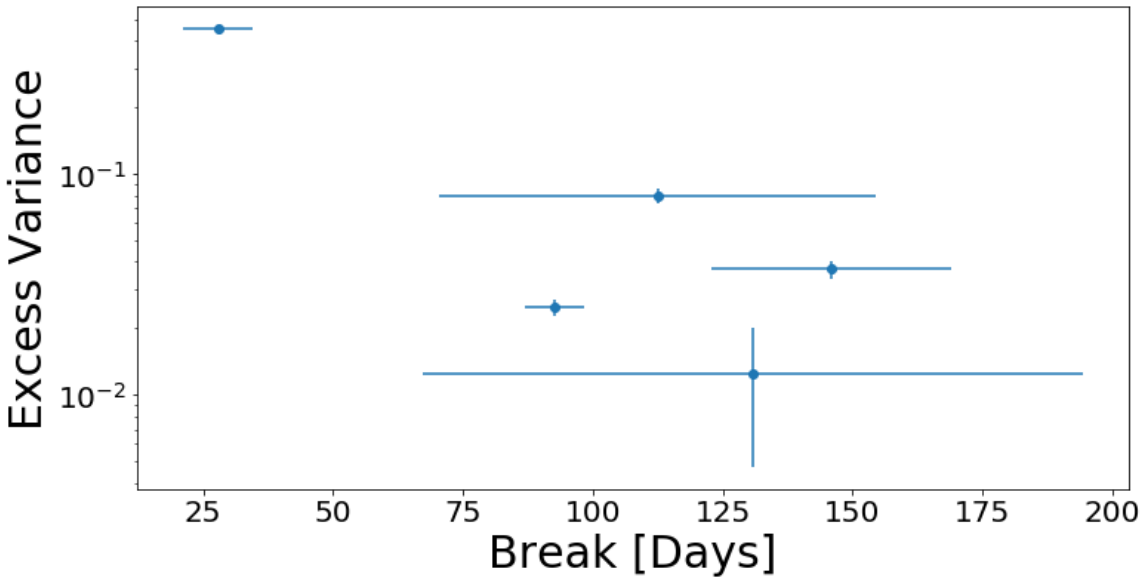

Figure 4.4: Plot showing the X-ray excess variance at half year intervals against the X-ray structure function break time in days.

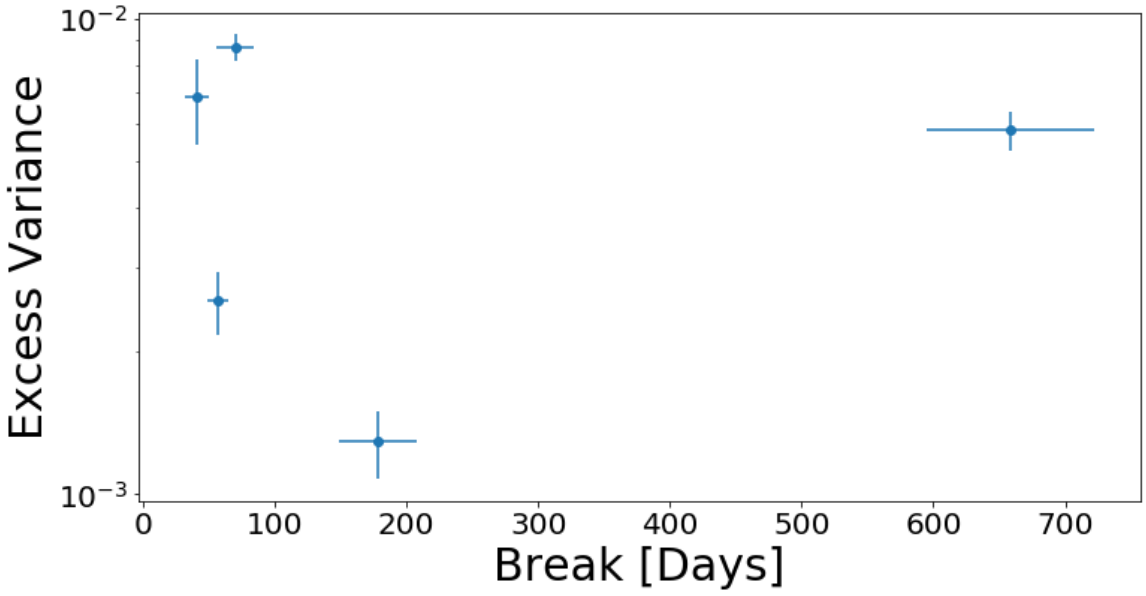

Figure 4.5: Plot showing the Radio excess variance at half year intervals against the Radio structure function break time in days. The outlier is NGC 1052.

Chapter 5

Conclusion

Given the correlations found between the structure function break time and a visual correlation between the values of the indices, it may be that the process creating the X-ray and Radio emission is the same process. There is no evidence of a time lag between the two regions that is within a 10 year time span. The propagation through the process in the jet perhaps may take a significant amount of time, so not finding a correlation between the light curves that falls in the 10 year time range is not unlikely if that were the case. Further research from this work may include expanding the archival data used in order to expand the length of the light curves to probe longer time scales. There is also the difference in variability that may come into effect. Comparing a highly variable X-ray light curve with a less variable Radio light curve may hide the overall correlation between the light curves due to the difference in variability. Applying some smoothing functions to the light curves to eliminate the shorter timescale variability to try and more clearly find a correlation at longer timescale may prove to be helpful.

In the structure functions parameters some correlations were found, and in these correlations there are some outliers. Due to the nature of the sources these outliers could indicate that the difference in the sources is what is being shown, or that due to the data quality some of the detail in the structure functions was not able to be

recovered as well as some other sources. The NGC 1052 structure function could show some break feature at the 100 day region but the breaks in the light curve may not allow this break to be seen as clearly. The Mrk 421 structure function does not extend to low time segments, stopping at about 10 days. Should the smaller timescale be probed, the initial index may change or remain different, perhaps differentiating the radio process or implying a secondary process is also present in this source that is different from the other sources.

The initial findings suggest an overarching process that probably appears in five sources presented in this work, and this process seems to be the same process in Radio and X-ray emission. There is evidence of discrepancies between some of the sources, which can be further probed with better data quality and longer light curves.

Bibliography

Roger Blandford, David Meier, and Anthony Readhead. Relativistic jets from active galactic nuclei. *Annual Review of Astronomy and Astrophysics*, 57(1):467–509, Aug 2019.

P. A. Evans, A. P. Beardmore, K. L. Page, J. P. Osborne, P. T. O'Brien, R. Willingale, R. L. C. Starling, D. N. Burrows, O. Godet, L. Vetere, and et al. Methods and results of an automatic analysis of a complete sample of swift-xrt observations of grbs. *Monthly Notices of the Royal Astronomical Society*, 397(3):1177–1201, Aug 2009.

P. A. Evans, A. P. Beardmore, K. L. Page, L. G. Tyler, J. P. Osborne, M. R. Goad, P. T. O'Brien, L. Vetere, J. Racusin, D. Morris, and et al. An online repository of swift/xrt light curves of $\vec{\gamma}$-ray bursts. *Astronomy and Astrophysics*, 469(1):379–385, Apr 2007.

L. C. Gallo, D. M. Blue, D. Grupe, S. Komossa, and D. R. Wilkins. Eleven years of monitoring the seyfert 1 mrk 335 with swift: Characterizing the x-ray and uv/optical variability. *Monthly Notices of the Royal Astronomical Society*, 478(2):2557–2568, May 2018.

Luigi C. Gallo. Revealing the innermost regions of active galaxies. *Journal of the Royal Astronomical Society of Canada*, 105(4):143–150, Aug 2011.

J. Y. Kim et al. Event horizon telescope imaging of the archetypal blazar 3c 279 at an extreme 20 microarcsecond resolution. *Astronomy and Astrophysics*, 640(A69): 21, 2020.

Alan P. Marscher. Relativistic Jets in Active Galactic Nuclei. In Philip A. Hughes and Joel N. Bregman, editors, *Relativistic Jets: The Common Physics of AGN, Microquasars, and Gamma-Ray Bursts*, volume 856 of *American Institute of Physics Conference Series*, pages 1–22, September 2006.

Bradley M. Peterson. Reverberation Mapping of Active Galactic Nuclei. *pasp*, 105: 247, March 1993.

Bradley M. Peterson. Measuring the masses of supermassive black holes. *Space Science Reviews*, 183(1):253–275, 2014.

G. Ponti, I. Papadakis, S. Bianchi, M. Guainazzi, G. Matt, P. Uttley, and N. F. Bonilla. Caixa: a catalogue of agn in the xmm-newton archive. *Astronomy & Astrophysics*, 542:A83, Jun 2012.

Joseph L. Richards, Walter Max-Moerbeck, Vasiliki Pavlidou, Oliver G. King, Timothy J. Pearson, Anthony C. S. Readhead, Rodrigo Reeves, Martin C. Shepherd, Matthew A. Stevenson, Lawrence C. Weintraub, and et al. Blazars in the fermi era: The ovro 40 m telescope monitoring program. *The Astrophysical Journal Supplement Series*, 194(2):29, May 2011.

Elizabeth Rivers, Alex Markowitz, and Richard Rothschild. Full spectral survey of active galactic nuclei in therossi x-ray timing explorerarchive. *The Astrophysical Journal*, 772(2):114, Jul 2013.

Ying Zu, C. S. Kochanek, and Bradley M. Peterson. An Alternative Approach to Measuring Reverberation Lags in Active Galactic Nuclei. *The Astrophysical Journal*, 735(2):80, July 2011.